Fuel 273 (2020) 117792

Contents lists available at ScienceDirect

Fuel

journal homepage: www.elsevier.com/locate/fuel

Full Length Article

Application of big data analysis technique on high-velocity airblast atomization: Searching for optimum probability density function

András Urbán[a], Axel Groniewsky[a], Milan Malý[b], Viktor Józsa[a,*], Jan Jedelský[b]

[a] Budapest University of Technology and Economics, Faculty of Mechanical Engineering, Department of Energy Engineering, 1111 Budapest, Műegyetem rkp. 3., Hungary
[b] Faculty of Mechanical Engineering, Brno University of Technology, Technicka 2896/2, 616 69 Brno, Czech Republic

ARTICLE INFO

Keywords:
Big data
Airblast
Rapeseed oil
PDA
Probability density function
Likelihood

ABSTRACT

In this paper, the droplet size distributions of high-velocity airblast atomization were analyzed. The spray measurement was performed by a Phase-Doppler anemometer at several points and different diameters across the spray for diesel oil, light heating oil, crude rapeseed oil, and water. The atomizing gauge pressure and the liquid preheating temperature varied from 0.3 to 2.4 bar and 25 to 100 °C, respectively. Approximately 400 million individual droplets were recorded; therefore, a big data evaluation technique was applied. 18 of the most commonly used probability density functions (PDF) were fitted to the histogram of each measuring point and evaluated by their relative log-likelihood. Among the three-parameter PDFs, Generalized Extreme Value and Burr PDFs provided the most desirable result to describe a complete drop size distribution. With restriction to two-parameter PDFs, the Nakagami PDF unexpectedly outperformed all the others, including Weibull (Rosin-Rammler) PDF, which is commonly used in atomization. However, if the spray is characterized by a single value, such as the Sauter Mean Diameter, i.e. an expected value-like parameter is of primary importance over the distribution, Gamma PDF is the best option, used in several papers of the atomization literature.

1. Introduction

The general behavior of a spray is well estimated by the average droplet size [1]; nevertheless, the size distribution is increasingly important in practical applications. The present study was motivated by liquid fuel combustion, where spray evaporation affects pollutant emissions [2]. Besides the analysis of the effect of atomizing air pressure on the spray, liquid preheating was also investigated in greater detail since highly viscous fuels, such as straight vegetable oils, approach the viscosity of conventional fossil fuels at around 100 °C [3]. The effect of liquid preheating on the Sauter mean diameter (*SMD*) was discussed in a previous paper [4]; currently, its impact on the droplet size distribution is evaluated. Beyond general-purpose painting [5], thin-films in e.g., fuel cell [6] and semiconductor technologies [7] are quite sensitive to the size distribution of a spray. The particle size in powder metallurgy is crucial since it affects the mechanical properties of the product [8] and the quality of surface treatment [9]. Besides the technical applications, the particle size determines the deposition characteristics of harmful materials [10] and inhalable drugs [11]. A uniform drop size distribution is of high importance for CO_2 capture efficiency in spray towers [12].

Several methods are available for spray droplet sizing [13]. In metallurgy, an electron microscope analysis is usually performed to study the size and shape of the resulting metal structure [14]. However, if the spray structure and its development are of primary importance, non-invasive imaging and light scattering techniques dominate [15]. The Phase Doppler technique is favorable for drop size spectra measurement as it offers a wide size dynamic range from microns to millimeters, high data rate, superior spatial resolution, and simultaneous droplet velocity data. Interferometric laser imaging for droplet sizing (ILIDS) can provide an instantaneous spatial distribution of droplet size [16]. However, the out-of-focus ILIDS technique does not allow dense spray measurement, which requires an additional in-focus imaging technique to resolve the droplet velocity, such as particle image velocimetry [17]. The laser diffraction-based method is widely used for rapid particle sizing since it is a robust technique to provide spray droplet size distributions in real-time but without velocity data. Since, in the present paper, a droplet size distribution analysis is performed for a wide range of conditions, the Phase Doppler technique was selected for the measurements.

A comprehensive study on water atomization was conducted by Xia et al. [18] in the low-velocity atomization region, which covers a different parameter range than that evaluated in the present paper. Kourmatzis et al. [19] investigated the effervescent atomization of

* Corresponding author.
E-mail address: jozsa@energia.bme.hu (V. Józsa).

https://doi.org/10.1016/j.fuel.2020.117792
Received 24 December 2019; Received in revised form 16 March 2020; Accepted 4 April 2020
Available online 09 April 2020

water with a particular emphasis on the methodology and data evaluation. Beyond research purposes, the established framework of ref. [19] can also be successfully used for the optimization of industrial atomizers [20]. Axial velocities and typical droplet sizes were investigated in the case of different air mixing ratio with the help of Phase Doppler Anemometry (PDA) by Chong and Hochgreb [21].

The governing physical laws of atomization were deeply investigated around the millennium. Lasheras et al. investigated the principles of air-assist atomization [22]. A successor work by Lasheras and Hopfinger [23] focused on liquid jet instability, and Varga et al. [24] proposed a formula to estimate the mean droplet diameter based on the ongoing physical processes. The ultimate goal was the prediction of the spray size distribution [25]. Liu et al. [26] used a stochastic model for predicting the size distribution of the spray by a prefilming airblast atomizer. Tharakan et al. [27] reviewed the available methods for spray modeling and concluded that the maximum entropy formulation is a promising approach. However, further research and validation are required before implementation to numerical codes. It was pointed out by Sovani et al. [28] that the spray formation is affected by multiple effects, considering only the relative velocity between the gas and liquid phases leads to false results. Gorokhovski and Saveliev [29] evaluated the airblast atomization and emphasized the log-normal droplet size distribution which was proposed by Kolmogorov. Several methods were tested for the estimation of *SMD* by the present authors [4] with a conclusion that the most general estimation technique for airblast atomization is based on a semi-empirical approach [30]. The superiority of empirical models over theoretical predictions probably stems from the highly non-equilibrium fluid dynamical and thermodynamical conditions involved in atomization.

There are various atomizer designs available for different purposes [1]. To better understand the atomization phenomena, the twin-fluid atomization [31] is a suitable method since the dependence of the spray is less affected by the actual atomizer geometry. In addition, the spray features a unimodal size distribution [23]. Due to its theoretical and practical relevance, an airblast atomizer was selected for the present analysis. It was developed in the ‘60 s [32] to provide a flexible solution for aviation to replace the pressure-swirl atomizers. This concept is still in use in modern aircraft burners [33]. Detailed mapping of a pintle injector was performed by Chen et al. [34]; it showed the complexity of the generated spray from the nozzle tip to the fully developed spray. If the evaluation is performed on large data sets, fundamental characteristics are difficult to derive. The size distribution of a developed spray is the sum of the results from various breakup mechanisms. These elementary processes were analyzed by Ghaemi et al. [35] for cold sprays, using an effervescent atomizer. The initial breakup of liquid jets was also evaluated by Lowe et al. [36] for both hot and cold conditions, focusing on the presence of droplets and ligaments in a wide range of conditions. The below discussed methodology can also be used for evaluating the primary breakup zone, which is a possible future direction of this research thread.

The scope of this paper is to determine the most suitable probability density functions (PDF) for high-velocity airblast atomization of different liquids in an extensive pressure and temperature range. The practical relevance of PDFs is that only a few parameters are required to describe the size distribution of a spray in a small volume. This is an advancement to *SMD* calculation since the spread of the droplet size is also available in addition to the mean value. Hence, with the key parameters available, a spray can be reconstructed and used for design and model development purposes. It was proven earlier by the authors [37] that few PDF types provide a good fit. Nevertheless, an exhaustive study on this topic is missing in the literature that characterizes a whole spray. This procedure offers a model to estimate the spatial characteristics and droplet size distribution of a spray. The proposed PDFs are the following. Generalized Extreme Value (GEV) is often used for the treatment of tail risks, e.g., in insurance [38] and finance [39]. In hydrology, the GEV distribution is applied to describe the annual maximum one-day rainfalls and river discharges [40]. This PDF can also be used in analyzing and predicting the weather in the future [41], the global temperature change [42], and atmospheric pollution analyses [43]. The Burr distribution can be used for analyzing human lifetime data [44]. The logistic distribution, in addition to sprays [45], is also used in politics [46], ocean biology [47], and in the evaluation of the mechanical properties of concrete [48]. The log-normal PDF is in use in scientometrics [49] and describing natural phenomena, such as the blood pressure of adults [50]. This PDF was also used by Lee and No [51] for droplet size prediction in a venture scrubber, by Li et al. [52] to characterize the secondary droplets formed during the impact of a droplet into a liquid film, by Lacour et al. [53] to evaluate the modes of a hollow-cone spray in crossflow, and by Feng et al. [54] in the droplet size distribution analysis of a high-pressure diesel oil spray. The Nakagami PDF is based on the log-normal PDF and was motivated by the measurement of high-frequency radio waves [55]. Recently, it has been used for studying the impact of fading channels on wireless communications [56]. The Rician PDF is used as the Euclidean norm of a bivariate normally distributed random vector. Its practical use can be found in wireless transmission modeling [57] and antenna design [58]. The Weibull PDF is the most common one in the atomization literature from among the proposed ones, which is the generalization of the Rosin-Rammler PDF. Applications involve, e.g., hydrology [59], wind speed distributions [60], particles generated by milling and crushing [61], and high-pressure water jet cleaning [62]. It is the most popular PDF in unimodal spray characterization, also used by Shafaee and Mahmoudzadeh [63] for airblast atomization.

Big data is most often characterized by volume, variety, velocity [64], and veracity [65], which refers to quantity, type, and nature of data, speed of data generation, and variety in data quality. With proper evaluation, they carry the possibility of deepening the global understanding of a system. Hence, this technique is used in several fields of engineering and is the engine of the fourth industrial revolution through the Industrial Internet of Things [66]. It helps in enhancing the manufacturing performance [67], scaling up to the whole production line [68], increasing transportation safety and sustainability [69]. In the energy industry, it has a leading role to optimize the solar power generation [70] and microgrid use [71] to promote efficient energy use [72].

Spray measurement does not bear all the characteristics of big data as it is performed only under pre-defined and well-controlled conditions. However, the evaluation techniques for small data cannot be used efficiently for millions of data points [73]. Consequently, big data visualization tools were used in the evaluation of PDA measurements to facilitate the recognition of patterns, trends, and correlations.

An in-depth investigation was performed by the authors earlier to find the most suitable estimation method for the *SMD* of the spray in a wide parameter range [4]. This paper is a follow-up, focusing on the PDF of the droplet sizes, measured at several points across the spray by using a PDA. The investigated conditions include several atomizing pressures, liquid preheating temperatures, and liquid types. Since the size distribution is approximated by several PDF types, even for airblast atomizers only, the goal of the present study is to perform an exhaustive analysis on PDF fitting. Besides the highly regular core, the distorted peripheral regions of the spray are also evaluated.

2. Experimental setup

The droplet size data sets were acquired by optical probing of spray produced by an airblast atomizer in the Spray laboratory at the Brno University of Technology. The following paragraphs describe the essential experimental equipment used, including the atomizer under test, the cold-spray test bench with the fluid supply system, and PDA.

The cross-section of the used plain-jet air blast atomizer is shown in Fig. 1. The inner diameter of the liquid pipe is 0.4 mm, where the low-velocity liquid flows through, and the high-velocity atomizing air

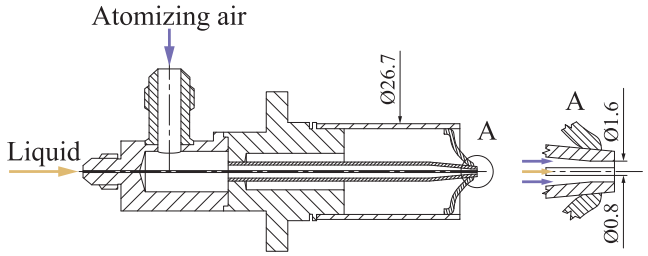

Fig. 1. Cross-section of the examined plain-jet airblast atomizer.

passes around the liquid channel concentrically. The atomizing medium and the liquid interact at the nozzle tip, leading to spray formation. Due to its simple design, this particular atomizer was extensively investigated in a pressurized environment [74], and in a micro gas turbine to evaluate liquid fuel combustion [75] and the effect of straight vegetable utilization on the combustion chamber [76]. This atomizer also provides a proper spray quality for atmospheric crude rapeseed oil combustion [77] with low pollutant emission.

The atomized liquids were standard diesel oil (D, EN 590), light heating oil (LHO), crude rapeseed oil (RO), and distilled water (W) at constant 0.35 g/s mass flow rate. Different liquids represent a wide viscosity range which facilitates the examination of various droplet size ranges. Typical droplet sizes were in the range of 5–30 μm, depending on the operation and material properties. The measured material properties of the investigated liquids were discussed in a previous work along with their uncertainties [4]. From a statistical point of view, this is of paramount importance for finding the most suitable PDF of the high-velocity airblast atomization.

The optical setup of the Fiber-based PDA (Dantec Dynamics A/S, Skovlunde, DK) is shown in Fig. 2 with an axial view to the spray, featuring measurement points along the X and Y directions. The two colors allowed for the simultaneous measurement of two velocity components. In the present case, the optical system was fixed, while a computer-controlled 3D traverse system positioned the atomizer.

A Spectra-Physics (CA, USA) Stabilite 2017 argon-ion laser produced a multi-line laser beam which was separated by a 60 × 41 transmitter into green and blue colors with wavelengths of 514.5 and 488 mm, respectively. The frequency shift of 40 MHz was performed by a Brag cell. A 57X50 fiber PDA receiver optics was used with a 112 mm diameter lens for spray detection. The focal length was 310 and 500 mm for the transmitting and receiving optics, respectively. The dimensions of the measurement volume were l_x = 0.60 mm, l_y = 0.072 mm, l_z = 0.073 mm in the coordinate system of Fig. 2.

The measured signals were processed by the BSA P80 flow and particle processor and visualized by BSA Flow Software v5.2. The maximum droplet size to measure was set to 64.1 μm with a size

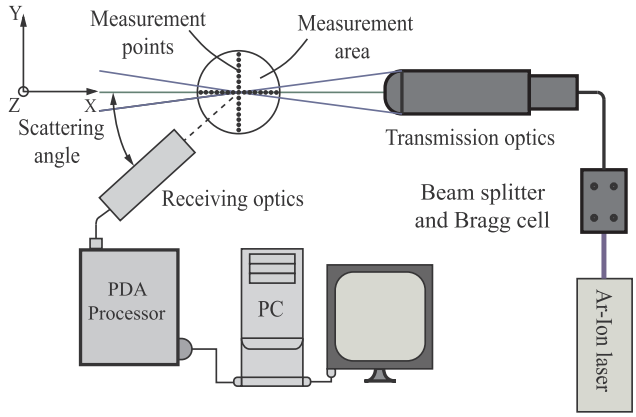

Fig. 2. Setup of the PDA system.

resolution of ± 0.05 μm. The PDA system was programmed to detect 40,000 individual droplets or record the data for 15 s, where the latter condition was necessary for the peripheral spray positions. According to a preliminary analysis of the velocity and *SMD* profiles, the results showed < 5% variation, and hence the spray is considered as axisymmetric [78]. The presented results are respective to a single ray (+X direction); however, the overall results of PDF fitting were closely identical for the other rays as well. The data points are referred to as *r*, which is the radius measured from the spray centerline. The deviation is attributed to the manufacturing defects, i.e., welding the ~200 mm long 0.8 mm diameter liquid pipe resulted in a small eccentricity. All the measurements were performed under atmospheric conditions.

The experimental test rig is shown in Fig. 3. The atomizing air was taken from the central compressed air system of the laboratory through a pressure regulator followed by a mass flow meter towards the atomizer. The following atomizing gauge pressures, p_g, were investigated: 0.3, 0.6, 0.9, 1.2, 1.8, and 2.4 bar. The lowest value was selected based on the criteria of stable combustion in the hot test cases – made without spray measurement – [77]. A pressurized tank was used to feed the liquids into the atomizer free of pressure fluctuations. A control valve and a Coriolis mass flow meter (Mass 2100 Di3 fitted with a Mass 6000 transmitter, Siemens AG, GE) were applied to set a constant 0.35 g/s liquid mass flow rate with an accuracy of ± 0.1% of the actual flow rate. A rotameter was also installed into the feed pipe for visual checking. Both liquid and atomizing air pipes were equipped with piezo-resistive pressure transducers DMP 331i (BD SENSORS s.r.o., CZ) and B class Pt100 resistance thermometers. Their uncertainties were 2 kPa and 0.3 °C, respectively. The range of the resulting air-to-liquid mass flow rate, *ALR*, was 0.78–2.07.

The liquid preheater was controlled by a PID unit, made by HAGA Kft., using a Pt100 for control. In addition, a toroidal transformer was used to set the heating power of the PID control to provide a smoother operation. The following preheating temperatures, t_p, were investigated for D, LHO, and RO: 25, 40, 55, 70, and 100 °C. W was an exception with a maximum temperature of 90 °C instead of 100 °C to avoid boiling.

The PDA measurements were carried out at three axial distances downstream of the nozzle, z = 20, 40, and 60 mm, with fifteen equally spaced radial points along X and Y axes at z = 60 mm, thirteen at z = 40 mm and seventeen at z = 20 mm. At z = 20 mm, the step was 1 mm between the points and 2 mm at z = 40 and 60 mm. Based on the analysis of the previous measurement results, the z < 20 mm region was later rejected [78] as droplet velocities in the vicinity of the nozzle tip exceeded ~300 m/s which is a limitation of the used PDA system.

All the conditions in terms of dimensionless numbers are discussed in Table 1. Since these numbers proved to be adequate for *SMD* estimation [4], no further temperature-related dimensionless number was added. Nevertheless, all of these numbers already contain material properties which are temperature-dependent.

ALR is the air-to-liquid mass flow ratio, $\mathrm{Re} = w_r \cdot d_0/\nu$ is the Reynolds number, $\mathrm{We} = w_R^2 \cdot d_0 \cdot \rho/\sigma$ is the Weber number, $\mathrm{Oh} = \sqrt{\mathrm{We}_L}/\mathrm{Re}_L$ is the Ohnesorge number, $\mathrm{Ma} = w/a$ is the Mach number, $MFR = \rho_A \cdot w_A^2/\rho_L \cdot w_L^2$ is the mass flux ratio while $EFR = \rho_A \cdot w_A^3/\rho_L \cdot w_L^3$ is the energy flux ratio. Subscripts *A* and *L* refer to air and liquid, respectively, which also refer to the used material properties in the dimensionless numbers. w_R is the relative velocity between the two jets, d_0 is the liquid jet diameter which is 0.4 mm, ν is the kinematic viscosity, ρ is the density, σ is the surface tension, and a is the local speed of sound. Since Re_L exceeded 10^6 in all the cases, the current conditions lie in the 'atomization' breakup regime, outside of the classical Oh-Re_L diagram, introduced by Ohnesorge [1]. According to Faeth et al. [79], the liquid jet breakup mode is the shear breakup due to the Oh < 0.5 and We_A > 200 range. The atomizing air has expanded at the nozzle and the discharge was adiabatic [78], and hence all of the air properties were calculated from adiabatic expansion of the pressurized, room-temperature atomizing air. The calculated discharge velocities varied

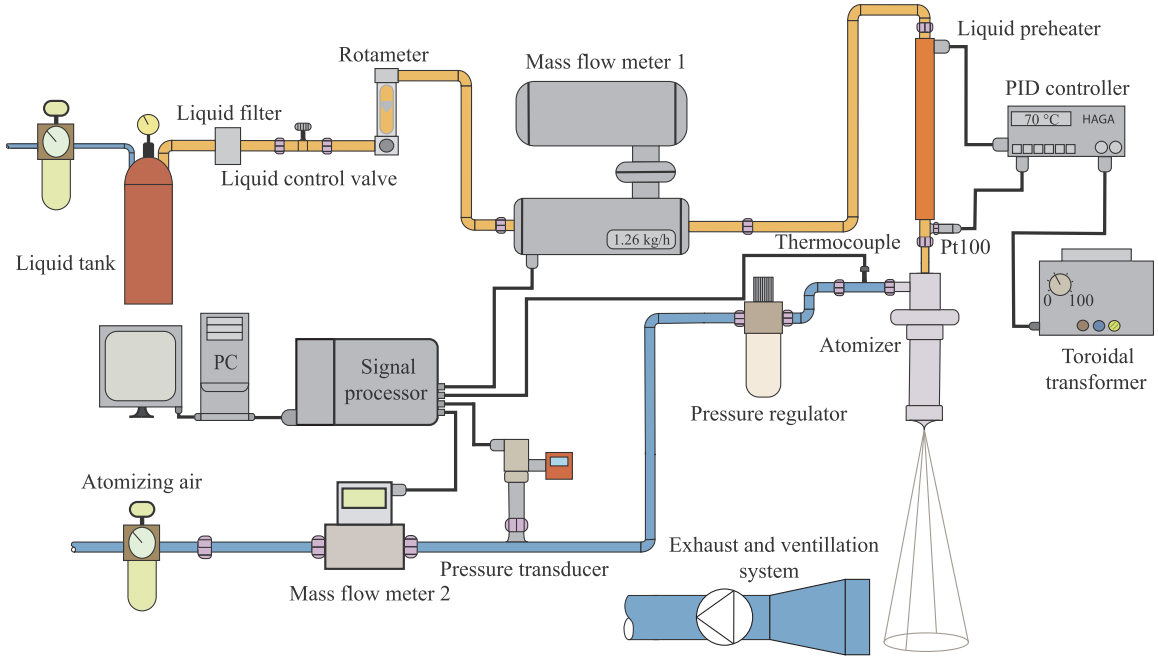

Fig. 3. Liquid and atomizing air piping and their instrumentation.

Table 1
Intervals of the investigation range of the liquids [4].

		D	LHO	RO	W
p_g [bar]	Min.	0.3	0.3	0.3	0.3
	Max.	2.4	2.4	2.4	2.4
ALR [–]	Min.	0.78	0.78	0.78	0.78
	Max.	2.07	2.07	2.07	2.07
Re_A [–]	Min.	8969	8974	8979	8994
	Max.	30,037	30,047	30,058	30,075
$Re_L/10^6$ [–]	Min.	22.7	5.04	1.57	91.2
	Max.	115.4	51.8	21.0	380
We_A [–]	Min.	988.4	792.5	730.6	289.7
	Max.	9549	4640	5014	1982
$We_L/10^6$ [–]	Min.	0.655	0.550	0.531	0.228
	Max.	4.64	2.35	2.63	1.16
Oh [–]	Min.	0.019	0.029	0.077	0.0028
	Max.	0.036	0.147	0.465	0.0052
Ma [–]	Min.	0.62	0.62	0.62	0.62
	Max.	1.45	1.45	1.45	1.45
MFR [–]	Min.	5.68	5.91	6.13	6.83
	Max.	31.7	33.23	34.8	37.7
EFR [–]	Min.	342.2	370.9	398	494.7
	Max.	4011	4401	4828	5667

between w_A = 208–420 m/s, according to p_g = 0.3–2.4 bar.

3. Methods

The raw measurement data samples were filtered, which is explained first. Secondly, the histogram creation is discussed which is essential for a significant reduction in the base data followed by the presentation of the investigated PDFs. Lastly, PDF mapping is detailed for big data visualization.

3.1. Data filtering

Over 400 million individual droplet data were generated during the measurement, which required quality control prior to the analysis. Firstly, the data outside of the physically rational measurement range was eliminated since the wavelength of the green laser beam can be considered as a lower boundary of sensing [80]. In the present case, nearly one percent of the droplet diameter data was below the 0.532 μm threshold value. In the next step, box plots were created for the remaining data, and the interquartile range (IQR; data range between 75th and 25th percentiles) was calculated. IQR was multiplied by 1.5; then above and below the resulting thresholds, the outlier data were permanently removed, which meant ~5% further data loss. This data filtering method is useful when the data is not normally distributed [81].

3.2. Visualization of the droplet size distribution

A convenient way of visualizing large datasets, where its size makes the interpretation difficult in a tabular form, and the individual points originated from the same process, is to create a histogram. Its abscissa contains the class intervals, or bins, frequently specified as consecutive, equally sized, non-overlapping ranges of a variable, while the ordinate contains the probability (frequency) of the data occurring in the dataset.

The nature of the distribution depends on the size of the bins [82], demonstrated by Szuwalski [83] through the analysis of crab molt sizes. There are several analytical procedures available to calculate the number of classes (k), based on the number of individual samples in the data (n). Brkić [84] proposed a square root and a logarithmic relationship. Since the number of measured data samples of a spray analysis is usually high, Rice Rule ($k = 2 \cdot n^{1/3}$) is suggested and was applied, which resulted in 1 μm bin size for all histograms of this study. Raw data in Fig. 4 shows the drop size histogram of a D spray at two p_g. At the same time, the other conditions were similar to demonstrate the characteristics of a regular histogram with four PDFs fitted, which is discussed in the next subsection. The *SMD* is also included in all histograms. The model fitting procedure was performed in Matlab using the fitdist function [81].

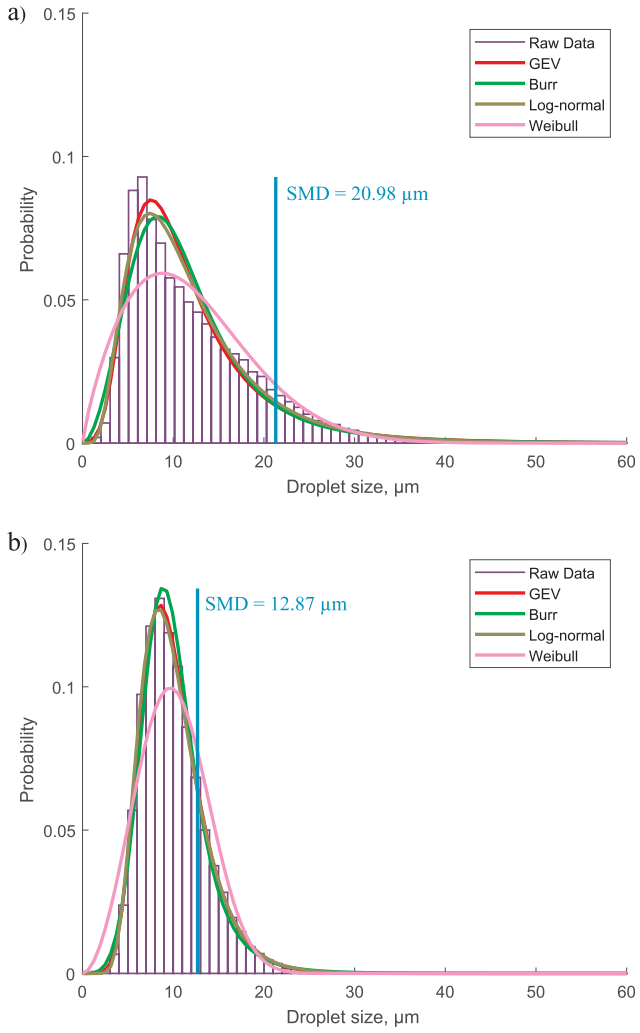

Fig. 4. Drop size histogram of D at t_p = 25 °C, r = 0 mm, z = 60 mm, and a) p_g = 0.3 bar, b) p_g = 2.4 bar.

3.3. Droplet size distribution functions

The droplet size distribution of a spray can be predicted if the shape of the PDF – fitted to the measured data – and its parameters are known. Depending on the characteristics of the atomization and of the droplet distribution, different types of models (fitted model provides the PDF) can lead to a reasonable approximation. The histogram of the droplet size distribution indicates that only positive, unimodal, and continuous PDFs can lead to sensible predictions. Also, a previous study [37] has shown that suitable PDFs require two or three parameters. Based on these criteria, 18 PDFs were investigated. These are as follows: Exponential, Gamma, Birnbaum-Saunders, Burr, Extreme Value, Generalized Extreme Value, Generalized Pareto, Half-normal, Log-logistic, Logistic, Log-normal, Nakagami, Normal, Rayleigh, Rician, Stable, t Location-Scale, and Weibull. Seven PDFs were superior over the others which are discussed further; they are the Burr (BU), the Generalized Extreme Value (GEV), the Logistic (LO), the Log-normal (LN), the Nakagami (NA), the Rician (RI), and the Weibull (WE; which is the generalized variant of the Rosin-Rammler PDF) respectively. They are all unimodal, two-parameter PDFs – GEV and BU have three-parameters –, which contain an exponential term, defined by Eqs. (1)–(7). Their parameters are noted with a, b, and c, while D refers to the droplet diameter. All the subscripts refer to the corresponding PDF listed above. Note that the below-presented performance maps for all the 18 PDFs are available as supplementary material of this paper.

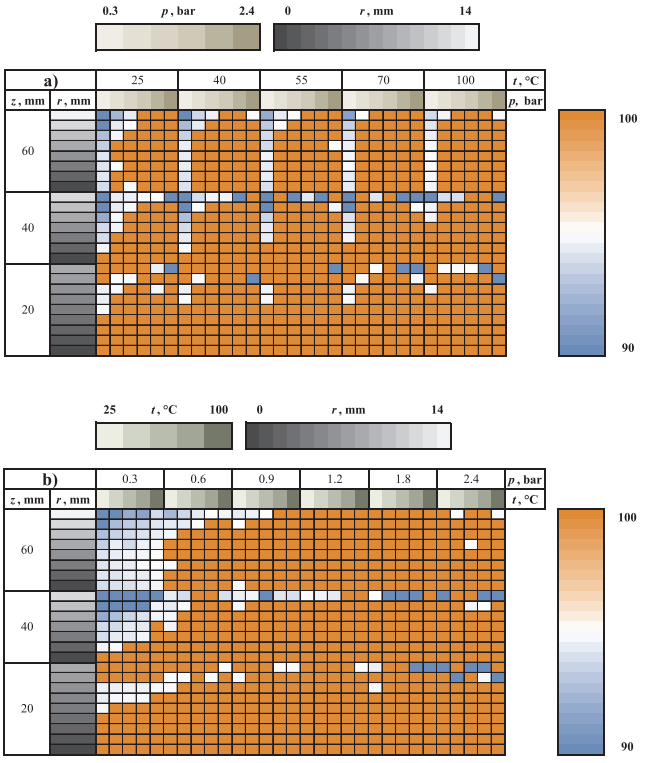

Fig. 5. Performance map of GEV for D. Results are ordered by a) t_p b) p_g.

$$f(D)_{BU} = (b_{BU}\cdot c_{BU}/a_{BU}\cdot(D/a)^{c_{BU}-1})/(1+(D/a_{BU})^{c_{BU}})^{b_{BU}+1} \quad (1)$$

$$f(D)_{GEV} = 1/b_{GEV}\cdot t(D)^{c_{GEV}+1}\cdot\exp(-t(D)) \quad (2)$$

$$t(D) = \begin{cases}(1+c_{GEV}\cdot((D-a_{GEV})/b_{GEV}))^{-1/c_{GEV}}, & \text{if } c_{GEV}\neq 0,\\ \exp(-(D-a_{GEV})/c_{GEV}), & \text{if } c_{GEV}=0\end{cases}$$

$$f(D)_{LO} = \exp(-(D-a_{LO})/b_{LO})/[b_{LO}\cdot(1+\exp(-(D-a_{LO})/b_{LO}))^2] \quad (3)$$

$$f(D)_{LN} = (1/(\mathrm{D}\cdot a_{LN}\cdot\sqrt{2\cdot\pi}))\cdot\exp(-(\ln D-b_{LN})^2/(2\cdot a_{LN}^2)) \quad (4)$$

$$f(D)_{NA} = 2\cdot(a_{NA}/b_{NA})a_{NA}\cdot[1/\Gamma(a_{NA})]\cdot D^{(2\cdot a_{NA}-1)}\cdot\exp(-a_{NA}\cdot D^2/b_{NA}) \quad (5)$$

$$f(D)_{RI} = D/a_{RI}^2\cdot\exp(-(D^2+b_{RI}^2)/(2\cdot a_{RI}^2))\cdot I_0(D\cdot b_{RI}/a_{RI}^2) \quad (6)$$

$$f(D)_{WE} = a_{WE}/b_{WE}\cdot(D/b_{WE})^{a_{WE}-1}\cdot\exp(-(D/b_{WE})^{a_{WE}}) \text{ for } D\geq 0 \quad (7)$$

Many calculations work with mean or average diameters, such as *SMD*, instead of the complete drop size distribution. If the goal is the prediction of the mean diameter, Gamma PDF outperforms the rest of the tested PDFs, as it was shown earlier [78]. However, it was outperformed by several PDFs in modeling the distribution; therefore, it is not discussed in the later parts of the paper. Also, previous experience [37] showed that the Nukiyama-Tanasava PDF is mathematically ineffective due to its non-predictable parameters; consequently, it was omitted from the present study.

3.4. PDF mapping

Maximum likelihood estimation is a method for fitting the equations to the data and comparing these equations to find the best one. The PDF with the highest log-likelihood (or lowest negative log-likelihood) predicts the probability of the droplet size most accurately, which was also calculated and stored by Matlab when the fitdist function was called. The best fit was calculated based on the maximum likelihood for all PDFs, excluding LN, which was fitted by calculating the square root of the unbiased estimate of the variance of the log of the data [81].

With different settings, overall 10,800 measurements were

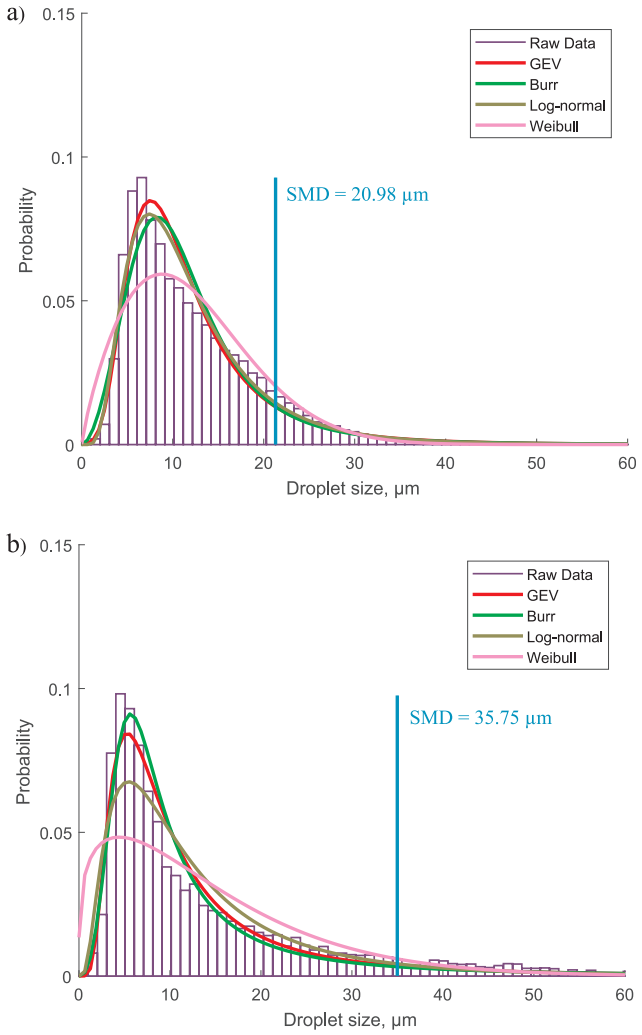

Fig. 6. PDF fit in the case of D at p_g = 0.3 bar, t_p = 25 °C, z = 60 mm, and a) r = 0 mm, b) r = 12 mm.

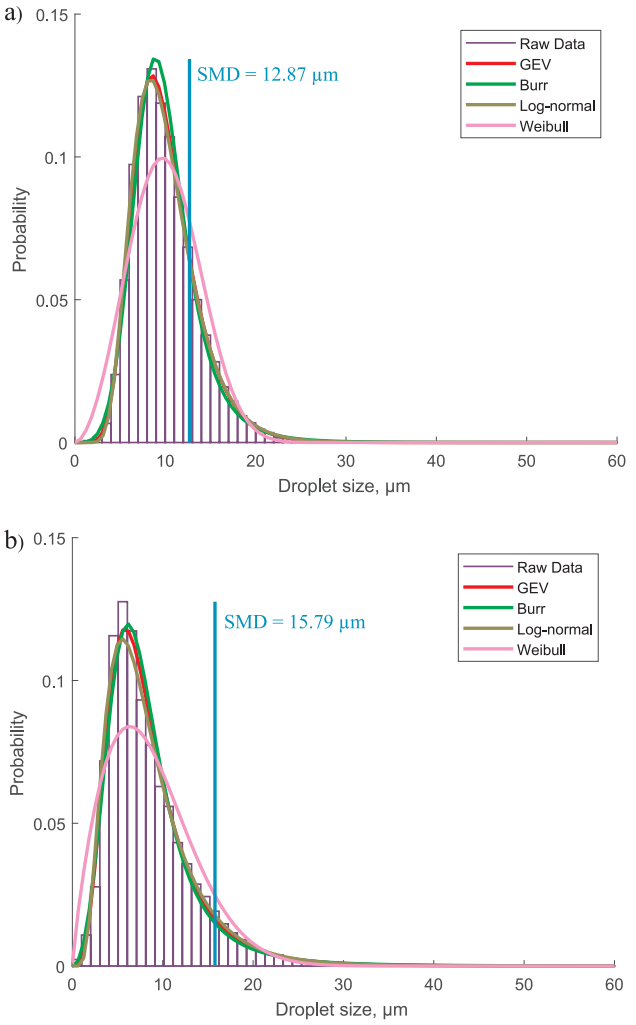

Fig. 7. Effect of viscosity in the case of a) D and b) RO at p_g = 2.4 bar, t_p = 25 °C z = 60 mm, r = 0 mm.

performed, and all 18 PDFs were fitted to each dataset and evaluated based on the likelihood estimation. The negative log-likelihood results were rescaled between 0 and 100, representing the performance of the functions relative to the worst and best performances, respectively. To evaluate the performance of the functions qualitatively, relative log-likelihoods were summarized in a color scale table for every PDF separately. The inclusion of all PDFs was necessary from the evaluation point of view since all the seven highlighted PDFs performed well at several points. Differentiating only between their performances would lead to highlighting the best one, resulting in the loss of valuable information about the physical phenomena. Since the measurement data always contain uncertainties, differentiating between excellently performing PDFs has no physical meaning.

Fig. 5 shows the performance map of GEV for D. Pressure and temperature conditions vary on the abscissa while axial and radial distances are indicated on the ordinate. The content of Fig. 5a is identical to 5b. In the former case, data is principally sorted by t_p to highlight the effect of p_g at a given t_p while Fig. 5b shows it in an inverted manner. At different radial distances, the performance map provides information on how accurately a PDF can predict the droplet size on the boundary, r = 8–14 mm, or in the core, r = 0–4 mm, while z shows the effect of the spray development, using a relative scale. Note that the relative log-likelihood is ranging from 90 to 100 for a better visual representation to enhance the recognition of patterns, trends, and correlations.

4. Results and discussion

This section is divided into two subsections where the local and global evaluation are both presented, following Figs. 4 and 5 of Section 3. Hence, Section 4.1 presents a few characteristic droplet size histograms and four selected PDFs fitted on them. It highlights the differences between D and RO atomization and the size distribution of the central and peripheral regions. In addition, the *SMD* is always indicated in the corresponding figures. Section 4.2 presents the overall evaluation based on the relative log-likelihood of selected PDFs for all the investigated setups. Note that all the performance maps of the seven highlighted PDFs are available as supplementary data of this paper.

4.1. Overview of histograms and probability density function fits

Fig. 6 compares a central and a peripheral histogram with four fitted PDFs in the case of D. The first three PDFs are included due to their excellent fit while WE was added as it is a widely used PDF in the literature of atomization. It can be seen that the histogram in the 0–10 µm range follows a similar trend. However, the peripheral region contains high number of larger droplets, exceeding 30 µm, see Fig. 6b, which are responsible for the nearly doubled *SMD* value. The analysis of their origin is not discussed here as it requires an in-depth analysis that is a subject of later research. Fig. 6a is similarly modeled by both GEV, BU, and LN, while the widely used WE notably falls behind them. The

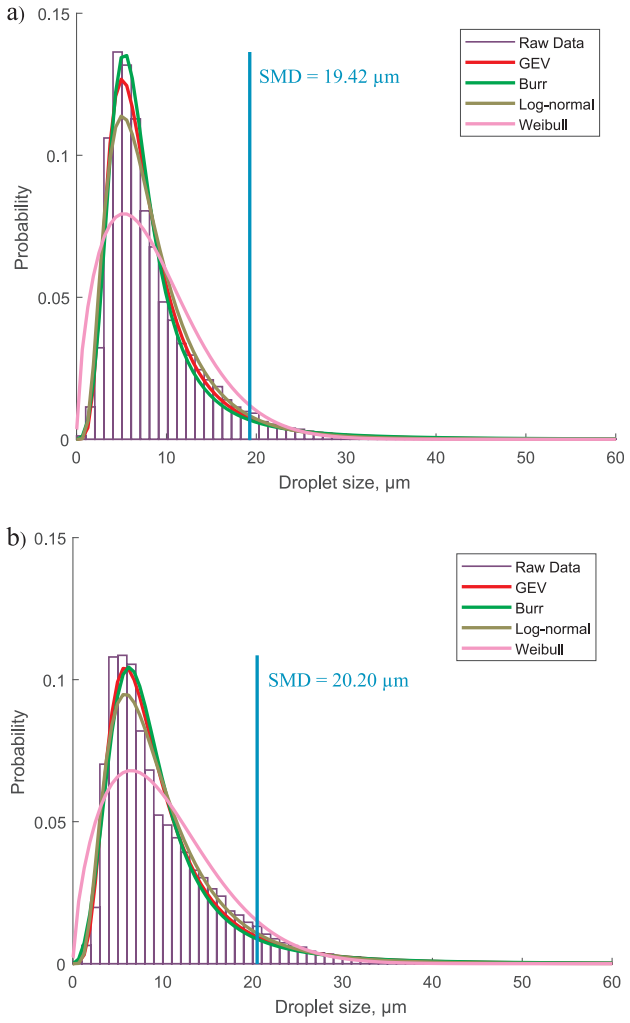

Fig. 8. Effect of preheating in the case of RO at p_g = 0.3 bar, t_p = a) 25 °C b) 100 °C z = 60 mm, r = 0 mm.

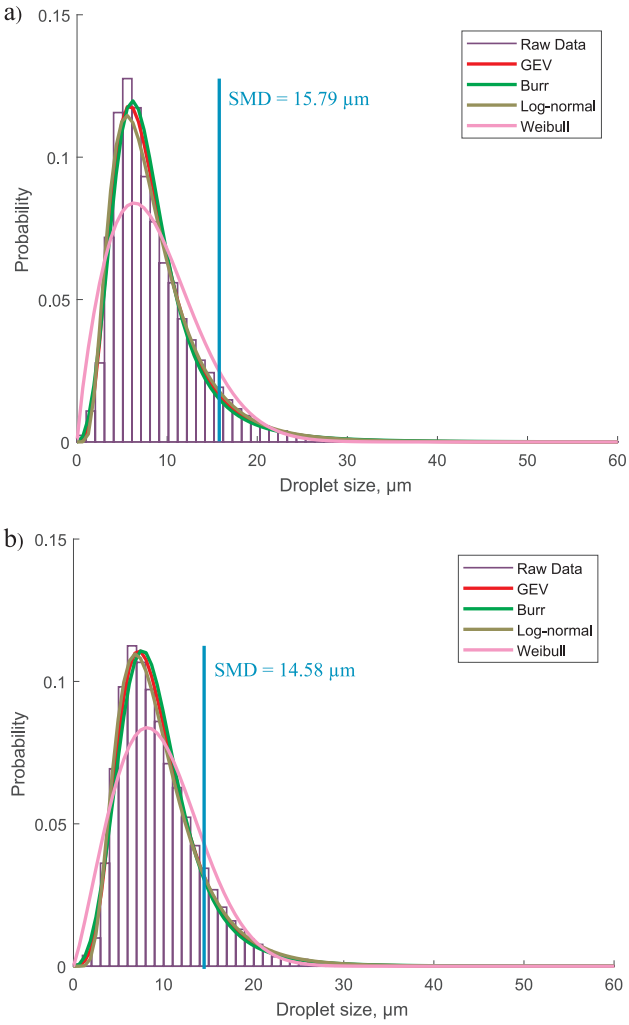

Fig. 9. Effect of preheating in the case of RO at p_g = 2.4 bar, t_p = a) 25 °C b) 100 °C z = 60 mm, r = 0 mm.

latter is an upper estimation in the 15–30 µm region, and it misses the peak. As it was mentioned, the irregular shapes of the histograms in the peripheral regions are expected to be the result of several droplet formation processes. Therefore, the fitted PDFs provide a relatively worse result than in the core. Nevertheless, the fit quality, evaluated in Section 4.2, shows it only on a relative scale.

Fig. 7 shows a comparison of RO and D under similar conditions in order to highlight the effect of viscosity on the spray size distribution. By comparing Figs. 6a and 7a, it can be seen that the peak slightly increases as p_g increases, which is a counterintuitive result. Nevertheless, the *SMD* is lower since the histograms of Fig. 6 contain a notable number of droplets above 20 µm while it is practically absent in the latter case. These characteristics can be qualitatively found when Fig. 7a and b are compared. Namely, the more viscous RO features a smaller peak droplet size than D while the larger sizes are present to a slightly greater extent. Therefore, the *SMD* of RO is higher than that of D, but the difference is small. Again, WE falls behind GEV, BU, and LN PDFs.

The lower t_p causes a lower standard deviation of the RO droplets around the mean, while the higher t_p generates a broader range of spread in the vicinity of the average, without changing the calculated *SMD* significantly. The low standard deviation of Fig. 8a indicates that the character of the drop size distribution of RO is more concentrated around 5 µm than that of Fig. 8b. In order to evaluate the effect of preheating, which was the highest for RO due to the significant drop in its viscosity, Fig. 8a and 8b show the histograms and PDFs at t_p = 25 and 100 °C. It is notable that the maximum probability since decreased from 0.13 to 0.11 as t_p was increased. Nevertheless, the maximum droplet size, which can be found in the spray, is slightly increased with the increasing temperature; meanwhile, the shape of the distributions is not changed. Further details on the effect of preheating on the droplet radial and axial velocity components and *SMD* are discussed previously [4] under the same conditions.

At higher pressures, the probability further decreases, which is introduced in Fig. 9a and b. Therefore, the preheating has a less significant effect on the shape and the parameters of each PDFs. Under this condition, the maximum droplet size does not change with t_p while *SMD* decreased. Meanwhile, this tendency was opposite at p_g = 0.3 bar, as shown in Fig. 8.

4.2. Evaluation of performance maps

Fig. 10 shows the results of the performance map of GEV, which provided the best fit at the majority of the measurement points. Hence, it scored the most 100 s in the relative log-likelihood scale. This PDF characterizes well the D atomization, which is followed by LHO, then RO that corresponds with their viscosity in ascending order. The fit quality of W is similar to D at z = 20 mm and to LHO at z = 40 and 60 mm. The performance is principally getting better with increasing p_g, although elevated t_p also has a beneficial effect in the case of all the investigated liquids, as shown in Fig. 10b. Considering the performance

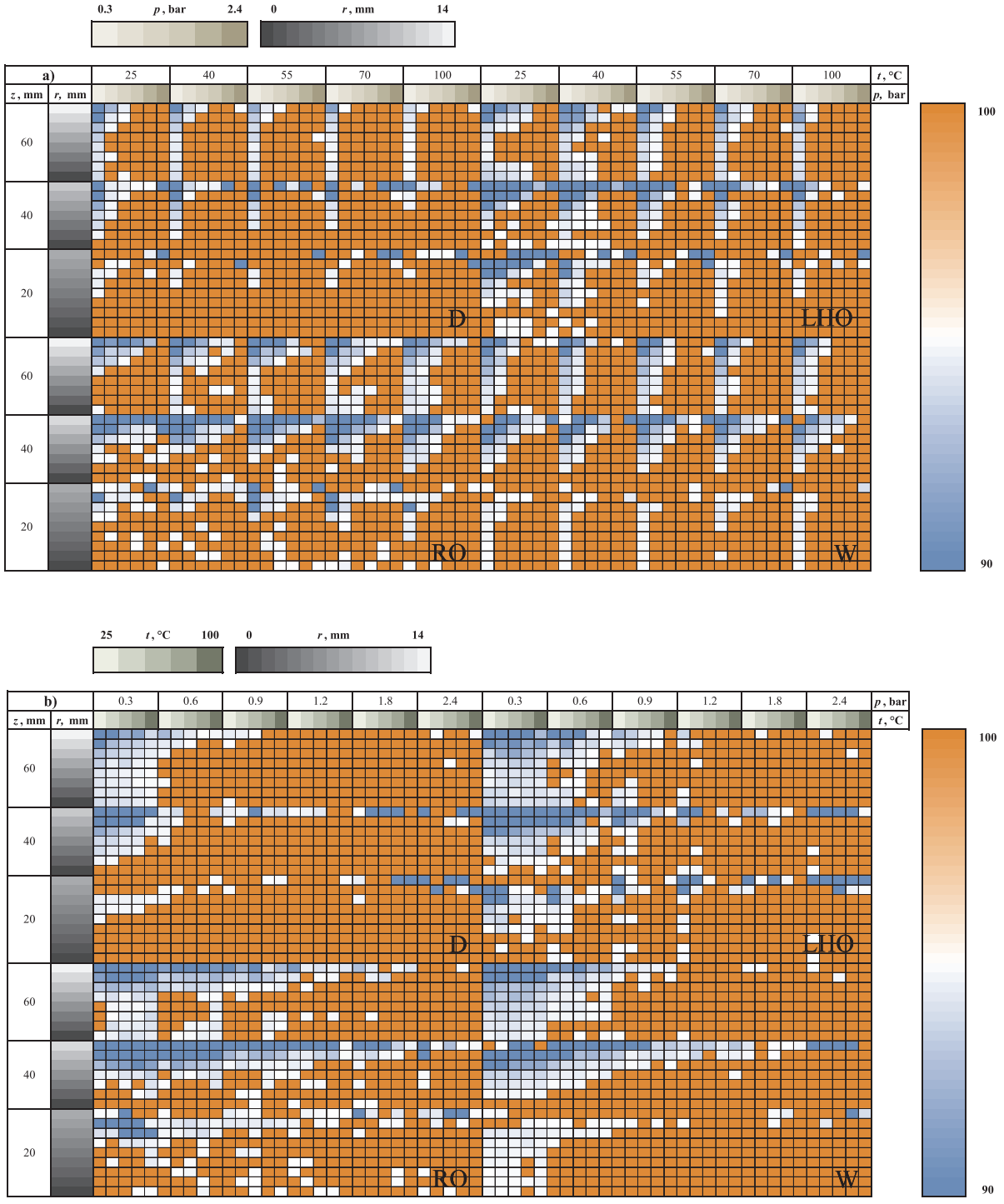

Fig. 10. Performance map of GEV for all liquids. Results are ordered by: a) t_p b) p_g.

as a function of r, it is getting worse towards the periphery region, which is more prevalent at $z = 40$ and 60 mm. In these regions, other PDFs provided notably better fits in the spray boundary. It can be explained by the mixed droplet sizes as the large droplets originate from the vicinity of the nozzle while the finer droplets went through further atomization.

Fig. 10a shows that the fit quality also increases with t_p, similarly to the effect of p_g in Fig. 10b. In the present case, p_g has a greater effect on the spray; hence, the evaluation through this parameter provides a better overview. At $z = 20$ mm, both D and W show regular droplet distributions up to $p_g = 1.2$ bar. As p_g keeps increasing, the residence time decreases as the convective effects increase with the increasing discharge velocity, leading to less regular size distributions, as shown in Fig. 10b. In these cases, liquid preheating may counteract this effect; however, it does not work for D, which already has low viscosity at room temperature. Apart from the peripheral regions and low p_g, GEV outperformed all the other PDFs for all liquids.

The BU PDF provided a better fit than GEV PDF at the peripheral region of the spray at lower p_g where the spray showed irregularity, see Fig. 11. Nevertheless, its fit at the core was also relatively good while its performance in the transitory regime, especially at low p_g, was low. Similar to the results of GEV, liquid preheating increases the fit quality.

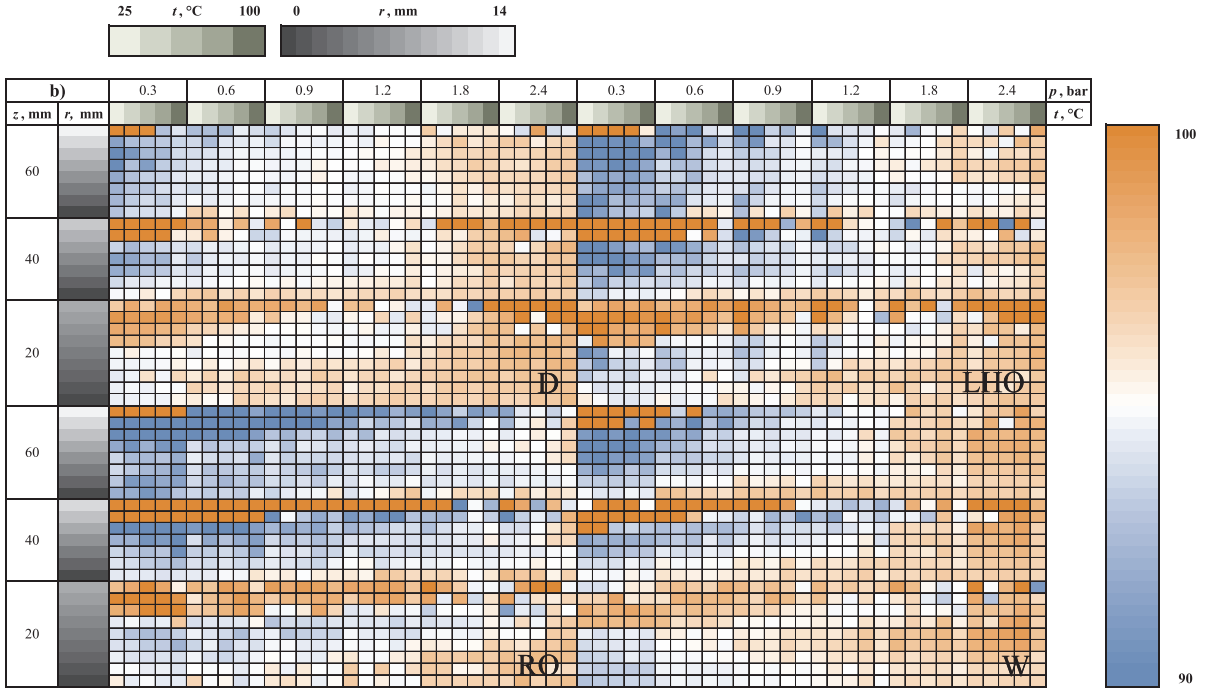

Fig. 11. Performance map of Burr for all liquids, ordered by p_g.

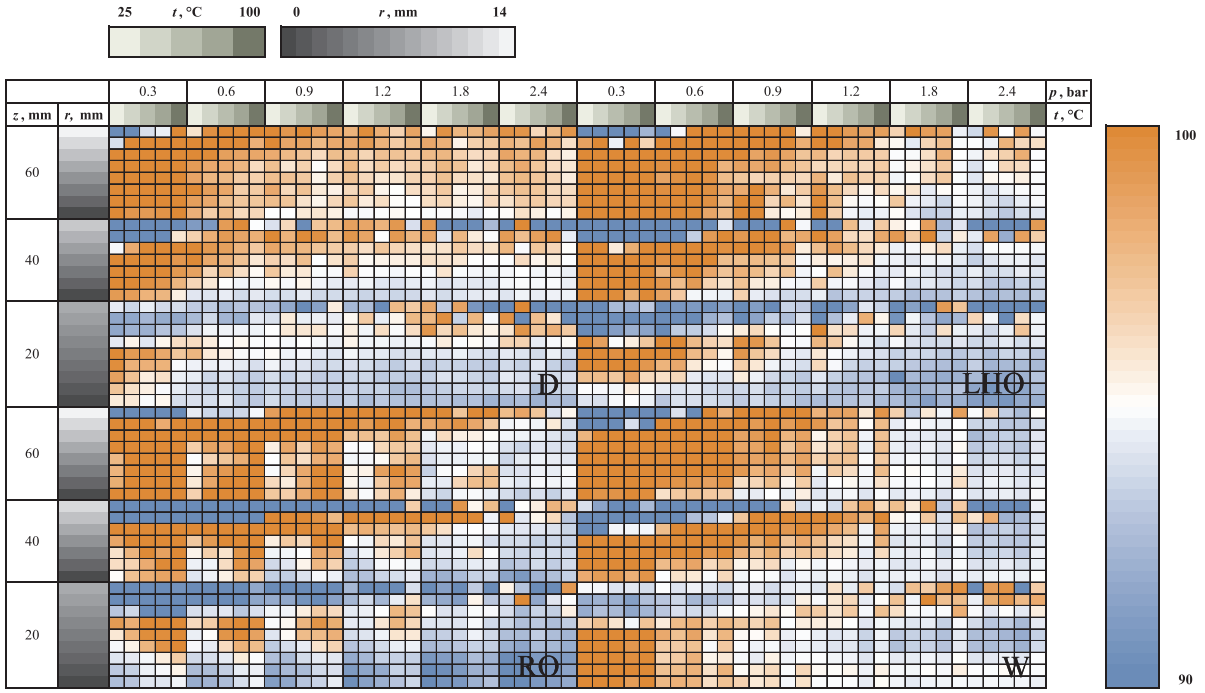

Fig 12. Performance map of Log-normal for all liquids. Results are ordered by p_g.

This PDF model the droplet size distribution of D and W better than that of LHO and RO. The relative fit quality decreases with the downstream distance from the nozzle, especially at low p_g. Increased t_p also leads to better fits; however, the effect of p_g is more pronounced.

Neither GEV nor BU PDFs were suitable for modeling the spray size distribution at $p_g = 0.3$ and 0.6 bar and distant points from the core. Under these conditions, the fit quality of LN surpassed all the others, especially for W and LHO, as shown in Fig. 12. The fit quality generally increased with z, and it provided a good fit for RO at $p_g \geq 0.9$ bar at $z = 60$ mm. In addition, the fit quality showed a low sensitivity on t_p.

Lastly, the WE PDF is presented in Fig. 13 due to its frequent use in atomization literature. Overall, this PDF behaves very much like GEV; nevertheless, the latter one is better in the majority of the cases. Hence, apart from a few exceptions, it is advised to use GEV instead of WE (or Rosin-Rammler) distribution for high-velocity airblast atomization.

To quantify the performance maps for the four investigated liquids, the average relative log-likelihoods are shown in Table 2. Due to the outstanding performance at the peripheral regions and good fits at the core, BU outperformed all the other functions in both the average value and the standard deviation of the relative log-likelihood analysis. The

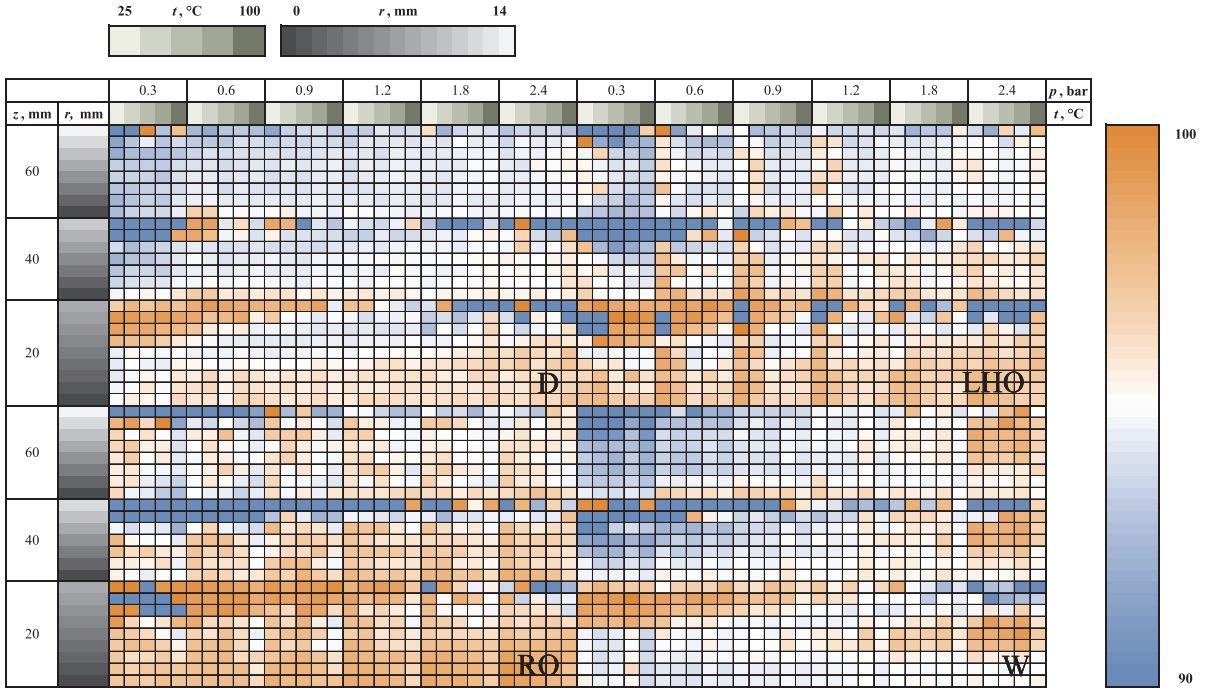

Fig 13. Performance map of Weibull for all liquids. Results are ordered by p_g.

Table 2
Performance map overall results. All the values are in percentages.

		GEV	Burr (BU)	Logistic (LO)	Log-normal (LN)	Nakagami (NA)	Rician (RI)	Weibull (WE)
D	Avg.	97.22	97.99	88.94	94.89	96.02	93.53	94.03
	Std. dev.	14.16	1.41	15.29	15.07	15.09	14.72	14.70
	100 s	80.97	4.03	0.28	8.47	3.47	0.28	0.28
LHO	Avg.	93.73	96.89	84.19	91.66	93.06	90.63	91.66
	Std. dev.	21.58	3.96	21.16	21.88	21.77	21.31	21.38
	100 s	64.58	7.08	0.00	17.22	8.06	0.00	0.56
RO	Avg.	93.21	96.16	83.13	91.03	92.97	90.34	91.89
	Std. dev.	22.78	4.26	21.67	22.57	22.58	22.14	22.25
	100 s	58.75	6.81	0.00	18.19	13.75	0.00	0.56
W	Avg.	95.36	97.68	86.31	93.57	94.38	91.84	92.69
	Std. dev.	18.87	2.07	19.03	19.09	19.00	18.49	18.60
	100 s	68.47	5.14	0.00	16.81	5.14	0.00	0.14

reason for this result is the poor performance of GEV at the spray periphery, even though this PDF outperformed the other ones in the spray core. The high standard deviation was also observed for the other PDFs, except for BU, which was characterized by a magnitude lower values. Apart from GEV and BU, which are the three-parameter PDFs, the NA distribution turned to be the best option from the two-parameter variants. Its performance is qualitatively similar to GEV and WE while the relative log-likelihood values fall between them. Note that the NA PDF is related to the Gamma distribution. Both RI and LO PDFs scored 100 in relative log-likelihood in only a few circumstances. Therefore, these PDFs can be omitted when the droplet size distribution of high-velocity airblast atomization is evaluated. As for the number of 100 s, GEV scored the majority of them in all the cases. It is followed by LN, NA, and only then by BU. Three other PDFs provided the best fit below 1% of the total number of cases.

5. Conclusions

The present paper discussed the global modeling of droplet size distribution functions by probability density functions (PDF) in the case of high-velocity airblast atomization, using big data evaluation techniques. The atomizing pressure, p_g, and the liquid preheating temperature, t_p, were varied, leading to a large parameter matrix. Four liquids were examined: water (W), standard diesel oil (D), light heating oil (LHO), and crude rapeseed oil (RO).

The key contribution of this work to the scientific literature is the quantitative analysis of several PDFs and the conclusion specifying ones that are the most suitable to model the droplet size distribution of airblast atomization. The core concept can be used in similar research works to reveal more details about spray characteristics. The results can be directly used for the development of numerical models for spray simulation. Based on the investigations, the following conclusions were derived.

1. General spray modeling by a single PDF is not possible since various regions feature various breakup modes. If outer regions of the spray and $p_g \leq 0.6$ bar conditions are omitted, the Generalized Extreme Value (GEV) PDF provided the best fit in terms of relative log-likelihood.
2. Burr PDF was the most suitable to model the spray characteristics since it worked well at the peripheral regions while it also provided a good estimation at the core. Hence, this PDF has the highest

average relative log-likelihood, considering all parameters.

3. Considering the two-parameter PDFs only, Nakagami (NA) is the best option among the five highlighted PDFs (note that both GEV and Burr PDFs have three parameters). NA and Weibull PDFs (the generalized form of Rosin-Rammler PDF) closely follow the qualitative results of GEV, while Weibull PDF is outperformed by NA under almost all conditions.
4. Lastly, the Log-normal PDF needs to be mentioned as it provided a good fit quality in the intermediate spray regions, at $p_g \leq 0.6$ bar, where the other superior PDFs have failed to perform well.
5. The remaining two PDFs, Rician and Logistic, performed well below the above mentioned five PDFs. Consequently, they are not suggested for characterizing the droplet size distribution of high-velocity airblast atomization. Even though the Weibull PDF is commonly used in the atomization literature, it is advised to prefer one of the three highlighted PDFs (GEV, Burr, and NA) over Weibull.

Funding

This work has been supported by the project №. GA18-15839S funded by the Czech Science Foundation and the project "Computer Simulations for Effective Low-Emission Energy Engineering" funded as project No. CZ.02.1.01/0.0/0.0/16_026/0008392 by Operational Programme Research, Development and Education, Priority axis 1: Strengthening capacity for high-quality research. (funding of the Czech researchers), National Research, Development and Innovation Fund of Hungary, project №. TUDFO/51757/2019-ITM Thematic Excellence Program and OTKA-FK 124704, New National Excellence Program of the Ministry for Innovation and Technology, project № ÚNKP-19-4-BME-213, and the János Bolyai Research Scholarship of the Hungarian Academy of Sciences (funding of the Hungarian researchers).

CRediT authorship contribution statement

András Urbán: Methodology, Software, Validation, Investigation, Writing - original draft, Visualization. **Axel Groniewsky:** Conceptualization, Methodology, Writing - original draft, Supervision. **Milan Malý:** Validation, Investigation. **Viktor Józsa:** Conceptualization, Writing - original draft, Writing - review & editing, Supervision, Project administration, Funding acquisition. **Jan Jedelský:** Resources, Writing - review & editing, Supervision, Funding acquisition.

Declaration of Competing Interest

The authors declare that they have no known competing financial interests or personal relationships that could have appeared to influence the work reported in this paper.

Appendix A. Supplementary data

Supplementary data to this article can be found online at https://doi.org/10.1016/j.fuel.2020.117792.

References

[1] Lefebvre AH, McDonell VG, Arthur H. Lefebvre VGM. Atomization and Sprays. Second. Boca Raton, FL, FL: CRC Press; 2017.
[2] Lefebvre AH, Ballal DR. Gas turbine combustion. Boca Raton: CRC Press; 2010. doi: 10.1002/1521-3773.
[3] Chiong MC, Chong CT, Ng JH, Lam SS, Tran MV, Chong WWF, et al. Liquid biofuels production and emissions performance in gas turbines: a review. Energy Convers Manag 2018;173:640–58. https://doi.org/10.1016/j.enconman.2018.07.082.
[4] Urbán A, Malý M, Józsa V, Jedelský J. Effect of liquid preheating on high-velocity airblast atomization: from water to crude rapeseed oil. Exp Therm Fluid Sci 2019;102:137–51. https://doi.org/10.1016/j.expthermflusci.2018.11.006.
[5] Schäfer W, Rosenkranz S, Brinckmann F, Tropea C. Analysis of pneumatic atomizer spray profiles. Particuology 2016;29:80–5. https://doi.org/10.1016/j.partic.2015.12.002.
[6] Bayer T, Selyanchyn R, Fujikawa S, Sasaki K, Lyth SM. Spray-painted graphene oxide membrane fuel cells. J Memb Sci 2017;541:347–57. https://doi.org/10.1016/j.memsci.2017.07.012.
[7] Madera RGB, Martinez MM, Vasquez MR. Fabrication of oxidized CuO and spray-pyrolyzed TiO 2 heterojunction thin film. Results Phys 2019;13. https://doi.org/10.1016/j.rinp.2019.102269.
[8] Nosko M, Štepánek M, Zifčák P, Orovčík L, Nagy Dvorák T, et al. Solid-state joining of powder metallurgy Al-Al2O3 nanocomposites via friction-stir welding: Effects of powder particle size on the weldability, microstructure, and mechanical property. Mater Sci Eng A 2019;754:190–204. https://doi.org/10.1016/j.msea.2019.03.074.
[9] Cheng KC, Chen JH, Stadler S, Chen SH. Properties of atomized AlCoCrFeNi high-entropy alloy powders and their phase-adjustable coatings prepared via plasma spray process. Appl Surf Sci 2019;478:478–86. https://doi.org/10.1016/j.apsusc.2019.01.203.
[10] Farkas Á, Lizal F, Elcner J, Jedelsky J, Jicha M. Numerical simulation of fibre deposition in oral and large bronchial airways in comparison with experiments. J Aerosol Sci 2019;136:1–14. https://doi.org/10.1016/j.jaerosci.2019.06.003.
[11] Lu W, Rades T, Rantanen J, Yang M. Inhalable co-amorphous budesonide-arginine dry powders prepared by spray drying. Int J Pharm 2019;565:1–8. https://doi.org/10.1016/j.ijpharm.2019.04.036.
[12] Cho M, Lee S, Choi M, Lee JW. Novel spray tower for CO2 capture using uniform spray of monosized absorbent droplets. Ind Eng Chem Res 2018;57:3065–75. https://doi.org/10.1021/acs.iecr.7b05309.
[13] Black DL, McQuay MQ, Bonin MP. Laser-based techniques for particle-size measurement: a review of sizing methods and their industrial applications. Prog Energy Combust Sci 1996;22:267–306. https://doi.org/10.1016/S0360-1285(96)00008-1.
[14] Ye X, Li Y, Ai Y, Nie Y. Novel powder packing theory with bimodal particle size distribution-application in superalloy. Adv Powder Technol 2018;29:2280–7. https://doi.org/10.1016/j.apt.2018.06.012.
[15] Tóth P, Brackmann C, Ögren Y, Mannazhi MN, Sepman A, Bengtsson PE, et al. Experimental and numerical study of biomass fast pyrolysis oil spray combustion: advanced laser diagnostics and emission spectrometry. Fuel 2019;252:125–34. https://doi.org/10.1016/j.fuel.2019.04.043.
[16] Kawaguchi T, Akasaka Y, Maeda M. Size measurements of droplets and bubbles by advanced interferometric laser imaging technique. Meas Sci Technol 2002;13:308–16. https://doi.org/10.1088/0957-0233/13/3/312.
[17] Hardalupas Y, Sahu S, Taylor AMKP, Zarogoulidis K. Simultaneous planar measurement of droplet velocity and size with gas phase velocities in a spray by combined ILIDS and PIV techniques. Exp Fluids 2010;49:417–34. https://doi.org/10.1007/s00348-009-0802-7.
[18] Xia Y, Khezzar L, Alshehhi M, Hardalupas Y. Droplet size and velocity characteristics of water-air impinging jet atomizer. Int J Multiph Flow 2017;94:31–43. https://doi.org/10.1016/j.ijmultiphaseflow.2017.04.014.
[19] Kourmatzis A, Lowe A, Masri AR. Combined effervescent and airblast atomization of a liquid jet. Exp Therm Fluid Sci 2016;75:66–76. https://doi.org/10.1016/j.expthermflusci.2016.02.002.
[20] Jedelský J, Jícha M. Spray characteristics and liquid distribution of multi-hole effervescent atomisers for industrial burners. Appl Therm Eng 2016;96:286–96. https://doi.org/10.1016/j.applthermaleng.2015.11.079.
[21] Chong CT, Hochgreb S. Effect of atomizing air flow on spray atomization of an internal-mix twin-fluid atomizer. At Sprays 2015;25:657–73. https://doi.org/10.1615/AtomizSpr.2015011361.
[22] Lasheras JC, Villermaux E, Hopfinger EJ. Break-up and atomization of a round water jet by a high-speed annular air jet. J Fluid Mech 1998;357:351–79. https://doi.org/10.1017/S0022112097008070.
[23] Lasheras JC, Hopfinger EJ. Liquid jet instability and atomization in a coaxial gas stream. Annu Rev Fluid Mech 2000;32:275–308. https://doi.org/10.1146/annurev.fluid.32.1.275.
[24] Varga CM, Lasheras JC, Hopfinger EJ. Initial breakup of a small-diameter liquid jet by a high-speed gas stream. J Fluid Mech 2003;497:405–34. https://doi.org/10.1017/S0022112003006724.
[25] Babinsky E, Sojka PE. Modeling drop size distributions. Prog Energy Combust Sci 2002;28:303–29. https://doi.org/10.1016/S0360-1285(02)00004-7.
[26] Liu H-F, Gong X, Li W-F, Wang F-C, Yu Z-H. Prediction of droplet size distribution in sprays of prefilming air-blast atomizers. Chem Eng Sci 2006;61:1741–7. https://doi.org/10.1016/j.ces.2005.10.012.
[27] Tharakan TJ, Mukhopadhyay A, Datta A, Jog MA, John Tharakan T, Mukhopadhyay A, et al. Trends in comprehensive modeling of spray formation. Int J Spray Combust Dyn 2013;5:123–80. https://doi.org/10.1260/1756-8277.5.2.123.
[28] Sovani SD, Sojka PE, Sivathanu YR. Prediction of drop size distributions from first principles: joint PDF effects. At Sprays 2000;10:587–602. https://doi.org/10.1615/atomizspr.v10.i6.40.
[29] Gorokhovski MA, Saveliev VL. Analyses of Kolmogorov's model of breakup and its application into Lagrangian computation of liquid sprays under air-blast atomization. Phys Fluids 2003;15:184–92. https://doi.org/10.1063/1.1527914.
[30] Lefebvre AH, Arthur H, Lefebvre. Airblast atomization. Prog Energy Combust Sci 1980;6:233–61. https://doi.org/10.1016/0360-1285(80)90017-9.
[31] Mlkvik M, Stähle P, Schuchmann HP, Gaukel V, Jedelsky J, Jicha M. Twin-fluid atomization of viscous liquids: The effect of atomizer construction on breakup process, spray stability and droplet size. Int J Multiph Flow 2015;77:19–31. https://doi.org/10.1016/j.ijmultiphaseflow.2015.06.010.
[32] Lefebvre AH, Miller D. The Development of an Air Blast Atomizer for Gas Turbine Application. CoA. Report Aero No. 193 June; 1966.
[33] Liu Y, Sun X, Sethi V, Nalianda D, Li YG, Wang L. Review of modern low emissions

combustion technologies for aero gas turbine engines. Prog Aerosp Sci 2017;94:12–45. https://doi.org/10.1016/j.paerosci.2017.08.001.
[34] Chen H, Li Q, Cheng P. Experimental research on the spray characteristics of pintle injector. Acta Astronaut 2019;162:424–35. https://doi.org/10.1016/j.actaastro.2019.06.032.
[35] Ghaemi S, Rahimi P, Nobes DS. Assessment of parameters for distinguishing droplet shape in a spray field using image-based techniques. At Sprays 2009;19:809–31. https://doi.org/10.1615/atomizspr.v19.i9.10.
[36] Lowe A, Kourmatzis A, Masri AR. Turbulent spray flames of intermediate density: Stability and near-field structure. Combust Flame 2017;176:511–20. https://doi.org/10.1016/j.combustflame.2016.10.024.
[37] Urbán A, Józsa V. Investigation of fuel atomization with density functions. Period Polytech Mech Eng 2018;62:33–41. https://doi.org/10.3311/PPme.11312.
[38] Guégan D, Hassani BK. A mathematical resurgence of risk management: an extreme modeling of expert opinions. Front Financ Econ 2014;11:25–45.
[39] Moscadelli M. The modelling of operational risk: experience with the analysis of the data collected by the basel committee. SSRN Electron J 2004. https://doi.org/10.2139/ssrn.557214.
[40] De Paola F, Giugni M, Pugliese F, Annis A, Nardi FGEV. Parameter estimation and stationary vs. non-stationary analysis of extreme rainfall in african test cities. Hydrology 2018;5:28. https://doi.org/10.3390/hydrology5020028.
[41] Kharin VV, Zwiers FW. Estimating extremes in transient climate change simulations. J Clim 2005;18:1156–73.
[42] Zwiers FW, Zhang X, Feng Y. Anthropogenic influence on long return period daily temperature extremes at regional scales. J Clim 2011;24:881–92. https://doi.org/10.1175/2010JCLI3908.1.
[43] Hazarika S, Borah P, Prakash A. The assessment of return probability of maximum ozone concentrations in an urban environment of Delhi: a Generalized Extreme Value analysis approach. Atmos Environ 2019;202:53–63. https://doi.org/10.1016/j.atmosenv.2019.01.021.
[44] Yari G, Tondpour Z. The new Burr distribution and its application. Math Sci 2017;11:47–54. https://doi.org/10.1007/s40096-016-0203-z.
[45] Massinon M, De Cock N, Forster WA, Nairn JJ, McCue SW, Zabkiewicz JA, et al. Spray droplet impaction outcomes for different plant species and spray formulations. Crop Prot 2017;99:65–75. https://doi.org/10.1016/j.cropro.2017.05.003.
[46] Gelman Andrew, Hill J. Data Analysis Using Regression and Multilevel/Hierarchical Models. New York Cambridge: Univ Press; 2007. p. 79–108.
[47] Lane J, Raimondi P, Kudela R. Development of a logistic regression model for the prediction of toxigenic Pseudo-nitzschia blooms in Monterey Bay, California. Mar Ecol Prog Ser 2009;383:37–51. https://doi.org/10.3354/meps07999.
[48] Burud NB, Chandra Kishen JM. Application of generalized logistic equation for b-value analysis in fracture of plain concrete beams under flexure. Eng Fract Mech 2019;210:228–46. https://doi.org/10.1016/j.engfracmech.2018.09.011.
[49] Thelwall M, Wilson P. Regression for citation data: An evaluation of different methods. J Informetr 2014;8:963–71. https://doi.org/10.1016/j.joi.2014.09.011.
[50] Makuch RW, Freeman DH, Johnson MF. Justification for the lognormal distribution as a model for blood pressure. J Chronic Dis 1979;32:245–50. https://doi.org/10.1016/0021-9681(79)90070-5.
[51] Lee SW, No HC. Droplet size prediction model based on the upper limit log-normal distribution function in venturi scrubber. Nucl Eng Technol 2019;51:1261–71. https://doi.org/10.1016/j.net.2019.03.014.
[52] Li J, Zhang H, Liu Q. Characteristics of secondary droplets produced by a single drop impacting on a static liquid film. Int J Multiph Flow 2019;119:42–55. https://doi.org/10.1016/j.ijmultiphaseflow.2019.06.015.
[53] Lacour SOL, Raoult F, Tinet C, Fournaison L, Delahaye A, Trinquet F. A modal analysis of the size distribution for an hollow-cone spray in cross-flow. Exp Therm Fluid Sci 2019;104:164–74. https://doi.org/10.1016/j.expthermflusci.2019.02.020.
[54] Feng Z, Tang C, Yin Y, Zhang P, Huang Z. Time-resolved droplet size and velocity distributions in a dilute region of a high-pressure pulsed diesel spray. Int J Heat Mass Transf 2019;133:745–55. https://doi.org/10.1016/j.ijheatmasstransfer.2018.12.147.
[55] Nakagami M. The m-distribution—A general formula of intensity distribution of rapid fading. Stat Methods Radio Wave Propag 2013:3–36. https://doi.org/10.1016/b978-0-08-009306-2.50005-4.
[56] Sanchez-Iborra R, Cano MD, Garcia-Haro J. Performance evaluation of QoE in VoIP traffic under fading channels. 2013 World Congr. Comput. Inf. Technol. WCCIT 2013, IEEE; 2013, p. 1–6. doi:10.1109/WCCIT.2013.6618721.
[57] Beaulieu NC, Hemachandra KT. Novel representations for the bivariate Rician distribution. IEEE Trans Commun 2011;59:2951–4. https://doi.org/10.1109/TCOMM.2011.092011.090171.
[58] Dharmawansa P, Rajatheva N, Tellambura C. New series representation for the trivariate non-central chi-squared distribution. IEEE Trans Commun 2009;57:665–75. https://doi.org/10.1109/TCOMM.2009.03.070083.
[59] Liu C, White RW, Dumais S. Understanding web browsing behaviors through Weibull analysis of dwell time. Proceeding 33rd Int. ACM SIGIR Conf. Res. Dev. Inf. Retr. - SIGIR '10, New York, New York, USA: ACM Press; 2010, p. 379. doi:10.1145/1835449.1835513.
[60] Kadhem AA, Wahab N, Aris I, Jasni J, Abdalla A. Advanced wind speed prediction model based on a combination of weibull distribution and an artificial neural network. Energies 2017;10:1744. https://doi.org/10.3390/en10111744.
[61] Brouwers HJH. Packing fraction of particles with a Weibull size distribution. Phys Rev E 2016;94:012905https://doi.org/10.1103/PhysRevE.94.012905.
[62] Gerhards C, Schramm M, Schmid A. Use of the Weibull distribution function for describing cleaning kinetics of high pressure water jets in food industry. J Food Eng 2019;253:21–6. https://doi.org/10.1016/j.jfoodeng.2019.02.011.
[63] Shafaee M, Mahmoudzadeh S. Numerical investigation of spray characteristics of an air-blast atomizer with dynamic mesh. Aerosp Sci Technol 2017;70:351–8. https://doi.org/10.1016/j.ast.2017.08.024.
[64] Laney D. 3D Data Management: Controlling Data Volume, Velocity, and Variety. 2001.
[65] Gantz J, Reinsel D. Extracting value from chaos. 2011.
[66] ur Rehman MH, Yaqoob I, Salah K, Imran M, Jayaraman PP, Perera C. The role of big data analytics in industrial internet of things. Futur Gener Comput Syst 2019;99:247–59. https://doi.org/10.1016/j.future.2019.04.020.
[67] Esmaeilian B, Behdad S, Wang B. The evolution and future of manufacturing: a review. J Manuf Syst 2016;39:79–100. https://doi.org/10.1016/j.jmsy.2016.03.001.
[68] Kozjek D, Vrabič R, Rihtaršič B, Butala P. Big data analytics for operations management in engineer-to-order manufacturing. Procedia CIRP 2018;72:209–14. https://doi.org/10.1016/j.procir.2018.03.098.
[69] Neilson A, Indratmo Daniel B, Tjandra S. Systematic review of the literature on big data in the transportation domain: concepts and applications. Big Data Res 2019;1:1–10. https://doi.org/10.1016/j.bdr.2019.03.001.
[70] Huang YF, Chang SH. Mining optimum models of generating solar power based on big data analysis. Sol Energy 2017;155:224–32. https://doi.org/10.1016/j.solener.2017.06.035.
[71] Moharm K. State of the art in big data applications in microgrid: a review. Adv Eng Informatics 2019;42:100945https://doi.org/10.1016/j.aei.2019.100945.
[72] Zhou K, Yang S. Understanding household energy consumption behavior: the contribution of energy big data analytics. Renew Sustain Energy Rev 2016;56:810–9. https://doi.org/10.1016/j.rser.2015.12.001.
[73] Faraway JJ, Augustin NH. When small data beats big data. Stat Probab Lett 2018;136:142–5. https://doi.org/10.1016/j.spl.2018.02.031.
[74] Nakamura S, McDonell V, Samuelsen S. The effect of liquid-fuel preparation on gas turbine emissions. J Eng Gas Turbines Power 2008;130:021506https://doi.org/10.1115/1.2771564.
[75] Bolszo CD. Investigation of Atomization, Mixing and Pollutant Emissions for a Microturbine Engine. UCI Undergrad Res J 2005;VIII:13–22.
[76] Prussi M, Chiaramonti D, Riccio G, Martelli F, Pari L. Straight vegetable oil use in Micro-Gas Turbines: system adaptation and testing. Appl Energy 2012;89:287–95. https://doi.org/10.1016/j.apenergy.2011.07.031.
[77] Kun-Balog A, Sztankó K. Reduction of pollutant emissions from a rapeseed oil fired micro gas turbine burner. Fuel Process Technol 2015;134:352–9. https://doi.org/10.1016/j.fuproc.2015.02.017.
[78] Urbán A, Zaremba M, Malý M, Józsa V, Jedelský J. Droplet dynamics and size characterization of high-velocity airblast atomization. Int J Multiph Flow 2017;95:1–11. https://doi.org/10.1016/j.ijmultiphaseflow.2017.02.001.
[79] Faeth GM, Hsiang LP, Wu PK. Structure and breakup properties of sprays. Int J Multiph Flow 1995;21:99–127. https://doi.org/10.1016/0301-9322(95)00059-7.
[80] Extension Of The Phase/Doppler Particle Analyzer To Submicron Particle Measurements 1985.
[81] MathWorks. MATLAB, Statistics Toolbox Release 2017a 2017.
[82] David M. Lane. Online Statistics Education: An Interactive Multimedia Course of Study (http://onlinestatbook.com/) 2007. http://onlinestatbook.com/2/graphing_distributions/histograms.html (accessed August 14, 2019).
[83] Szuwalski CS. Biases in biomass estimates: the effect of bin width in size-structured stock assessment methods. Fish Res 2016;180:169–76. https://doi.org/10.1016/j.fishres.2015.06.023.
[84] Brkić DM. A method for evaluation of number class intervals of histogram. Microelectron Reliab 1991;31:245–8. https://doi.org/10.1016/0026-2714(91)90206-M.